Environ. Sci. Technol. **2004**, *38,* 2813−2821

Historical Variations in the Stable Isotope Composition of Mercury in Arctic Lake Sediments

TOGWELL A. JACKSON* AND DEREK C. G. MUIR

Aquatic Ecosystem Protection Research Branch, National Water Research Institute, Environment Canada, 867 Lakeshore Road, P.O. Box 5050, Burlington, Ontario L7R 4A6, Canada

WARWICK F. VINCENT

Centre d'Études Nordiques, Université Laval, Québec, Québec G1K 7P4, Canada

The stable isotope composition of mercury (Hg) in a dated core from the anoxic zone of a saline, meromictic Arctic lake was found to vary as a complex function of the age and chemical composition of the sediment. Throughout the stratigraphic sequence, which spans the years 1899−1997, the ratios ^{198}Hg/^{202}Hg, ^{199}Hg/^{202}Hg, ^{200}Hg/^{202}Hg, ^{201}Hg/^{202}Hg, and ^{204}Hg/^{202}Hg expressed as δ-values (per mil deviations relative to a standard) reveal enrichment in ^{198}Hg, ^{199}Hg, ^{200}Hg, and ^{201}Hg, with depletion in ^{204}Hg, the degree of enrichment varying inversely with atomic mass. A plot of δ^{198}Hg, δ^{199}Hg, δ^{200}Hg, and δ^{201}Hg against depth gave parallel profiles characterized by large, regular undulations superimposed on an overall trend toward increase with depth (i.e. age), and the δ^{204}Hg profile is a mirror image of them. The δ^{198}Hg, δ^{199}Hg, δ^{200}Hg, and δ^{201}Hg values of the oldest (1899−1929) strata vary *inversely* with $NH_2OH{\cdot}HCl/HNO_3$-extractable manganese concentration, but those of the youngest (1963−1997) strata give a *positive* correlation; intermediate (1936−1956) strata show no correlation and negligible variation in δ-values, possibly signifying a transition phase in which the two opposite trends offset each other. The δ-values show similar but weaker relationships with organic carbon. The results strongly suggest fractionation of Hg isotopes by microbial activities linked to oxidation−reduction reactions in the lake, although effects of isotopic signatures indicative of the sources of the Hg have not been ruled out. The radical change in the nature of the relationship between δ-values and sediment chemistry over time may reflect environmental and biotic changes that altered the isotope-fractionating processes. These findings imply that variations in the isotopic makeup of Hg, together with related physical, chemical, and biological data, could yield important new information about the biogeochemical cycle of Hg.

Introduction

Contamination of aquatic environments with mercury (Hg) by atmospheric and aqueous transport from anthropogenic and natural sources, followed by accumulation of the Hg in sediments and biota, is a serious worldwide problem (*1*−*3*). Any systematic temporal or spatial variations in the stable isotope composition of this Hg could provide valuable information on the sources and biogeochemical cycling of the Hg, but until recently (*4*) there was no recorded evidence for their existence, and no indication that the subject had ever been researched. The stable isotopes of Hg (^{196}Hg, ^{198}Hg, ^{199}Hg, ^{200}Hg, ^{201}Hg, ^{202}Hg, and ^{204}Hg) (*5*) have been fractionated experimentally (*6*−*8*), implying that they may be subject to fractionation by natural and industrial processes. If so, we can expect to find systematic variations in the isotopic makeup of Hg in natural environments, including historical changes preserved in sediment sequences.

However, the possibility that the proportions of the stable isotopes of Hg vary significantly in nature has rarely been investigated. Evidence for natural fractionation of Hg isotopes has been found in Hg ores (*9*−*11*) and in meteorites and moon rocks (*12*−*14*), and, although doubts about these findings have been raised (*15*), the existence of differences in Hg isotope content among samples of Hg ore from different sources has been confirmed (*16*). Yet comparison of coal and fly ash samples yielded negative results (*17*). The first published evidence for fractionation of stable isotopes of Hg in an ecosystem was obtained by analysis of a core and assemblage of food web animals from Lake Ontario (*4*). This work provoked lively debate (*15*, *17*−*19*), in large part because the isotope analyses were done by quadrupole inductively coupled plasma mass spectrometry (Q-ICP-MS), which is less precise than more advanced techniques.

Here we present results of research employing multi-collector inductively coupled plasma mass spectrometry (MC-ICP-MS) to measure variations in the stable isotope composition of Hg in a sediment core from an Arctic lake. MC-ICP-MS is the most precise method of mass spectrometry and hence the method of choice for heavy elements such as Hg (*16*). As far as we know, our work was the first application of this powerful technique to the investigation of the isotopic makeup of Hg in an ecosystem. Our purpose was to determine whether the isotope composition of Hg in the core showed significant nonrandom historical variations, and, if so, whether these variations were attributable to preservation of isotopic signatures inherited from the sources of Hg contamination or to isotope fractionation in the environment, or both.

Materials and Methods

The core was taken from Romulus Lake, a small oligotrophic, saline, meromictic lake in the High Arctic desert of the Fosheim Peninsula of Ellesmere Island, Nunavut, Canada (*20*) (Figure 1) in May, 2000. Because it was known to have a high sedimentation rate, this lake had been selected as one of the field sites in a larger investigation of atmospheric Hg deposition in remote Northern lakes (*21*).

Many short, ephemeral streams flow into Romulus Lake, mainly during the brief season of melting snow, and runoff is enhanced by the presence of an impervious layer of permafrost a short distance below the ground surface (*20*). The local climate is arid owing to the rain shadow effect of nearby mountains, and, as it is also frigid, more than half of the limited annual precipitation is in the form of snow (*20*). In the drainage basin of the lake aeolian erosion of rocks and soil is an important process, salt crusts are ubiquitous on the ground, and the vegetation, which consists mainly of prostrate willows (*Salix arctica*) and grasses, is sparse (*20*). The local bedrock is made up of poorly consolidated sandstones,

* Corresponding author phone: (905)336-4795; fax: (905)336-6430; e-mail: t.a.jackson@ec.gc.ca.

10.1021/es0306009 CCC: $27.50 © 2004 American Chemical Society
Published on Web 04/08/2004

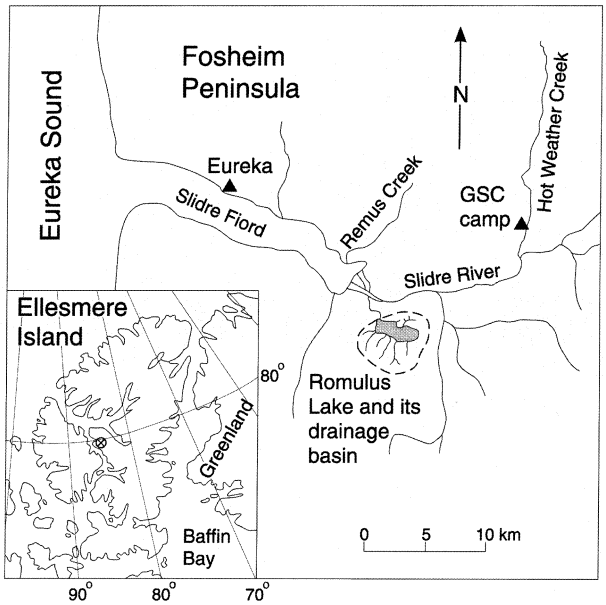

FIGURE 1. Map showing the location of Romulus Lake and its drainage basin (area bounded by dashed line).

siltstones, and coal underlying surficial deposits of till, marine silt, and fluvial sand and gravel (*20*). As there have been no human activities in or near the drainage basin other than those associated with a Geological Survey of Canada (GSC) station and a weather station (Eureka) located ~11 and 16 km, respectively, from the basin's periphery (Figure 1), all or most of the anthropogenic Hg in the lake is attributable to long-range atmospheric transport from industrial sites (e.g. coal-burning power plants) and population centers far to the south (*2, 3, 21−24*). Inputs of naturally occurring Hg probably consist of trace quantities from diffuse sources and scattered point sources (e.g. volcanoes) (*2, 3*). At the sampling site the water is 48 m deep and is perennially anoxic below the chemocline (*20*). The sediments in the anoxic zone consist of laminated clay, silt, and fine sand with alternating black and olive-brown laminae (*20*). Measurements made in the field showed that the bottom water had a pH of ~7, a specific conductivity of ~100 mS·cm^{-1}, an alkalinity of ~870 mg·L^{-1}, and a dissolved oxygen (O_2) content of 0 mg·L^{-1}.

The core was cut into 1 cm sections, which were freeze-dried. Total Hg analyses were performed by digestion with HNO_3/HCl (*aqua regia*) at 120 °C, addition of HNO_3, HCl, and $KMnO_4$, treatment with $SnCl_2$ to reduce dissolved Hg(II) to gaseous Hg(0), and measurement of Hg(0) levels in triplicate by cold vapor atomic absorption spectrometry using a Perkin-Elmer Flow Injection Mercury System. The stable isotopes of Hg in the sample extracts were determined with an automated, computerized ThermoFinnigan Neptune MC-ICP-MS unit employing argon (Ar) as the carrier gas and Faraday cups as the detectors. Following reduction of the dissolved Hg(II) to Hg(0) gas by online treatment with $SnCl_2$, the Hg(0), and associated solution were entrained by a stream of Ar, and the Hg(0) was stripped from the liquid phase in a liquid−gas separator (nebulizer) and injected into the plasma of the MC-ICP-MS unit by the Ar. The flow rates of the gas were 1.2 L·min^{-1} for sample gas, 1.3 L·min^{-1} for auxiliary gas, and 15 L·min^{-1} for cool gas, and the radio frequency (RF) power was 1300 w. Hg isotope concentrations were measured simultaneously using a separate Faraday cup for each isotope, and the Faraday cups were arranged in such a way as to avoid overlap of Hg isotope peaks by adjacent peaks. A standard solution of Hg in 3.5% HNO_3 (lot S-HG02027, Inorganic Ventures Inc.) was analyzed before and after every batch of five sample extracts, and, on completion of the run, extracts of three reference materials were analyzed: forest soil from Québec (sample SO-2, Canada Centre for Mineral and Energy Technology) and soil and copper-mill heads from Utah (samples GXR-2 and GXR-4, respectively, U.S. Geological Survey). Before the sample and standard solutions were analyzed, their Hg content was adjusted to the range 3−5 ng·mL^{-1} to ensure an acceptable degree of precision (better than 0.01%) while obviating the memory effects and excessively long washout times which ensue when Hg levels are too high. (If the initial Hg concentration was > 5 ng·nL^{-1}, it was lowered to ~5 ng·mL^{-1} by dilution; all other Hg levels fell in the range 3−5 ng·mL^{-1}.) The Hg content of the blank was < 40 pg·mL^{-1}. Each solution was automatically analyzed for Hg isotopes 25 times in rapid succession (using ^{206}Pb and ^{195}Pt measurements to correct for interference between ^{204}Pb and ^{204}Hg, and between ^{196}Pt and ^{196}Hg, respectively), and the mean and standard deviation of the measurements were calculated. Immediately afterward the system was rinsed out until the rinsings gave the same instrument readings as the blank, signifying that it was ready to analyze another solution. The raw isotope data were expressed as the ratios ^{196}Hg/^{202}Hg, ^{198}Hg/^{202}Hg, ^{199}Hg/^{202}Hg, ^{200}Hg/^{202}Hg, ^{201}Hg/^{202}Hg, and ^{204}Hg/^{202}Hg, and the per mil (‰) deviations of the sample ratios from the standard ratios (i.e. the δ^{196}Hg, δ^{198}Hg, δ^{199}Hg, δ^{200}Hg, δ^{201}Hg, and δ^{204}Hg values) were calculated using the formula $\delta^{X}\mathrm{Hg} = [(^{X}\mathrm{Hg}/^{202}\mathrm{Hg})_{\mathrm{sample}} - (^{X}\mathrm{Hg}/^{202}\mathrm{Hg})_{\mathrm{standard}}]\cdot 10^{3}/(^{X}\mathrm{Hg}/^{202}\mathrm{Hg})_{\mathrm{standard}}$, where $X = 198$, 199, 200, 201, or 204, to correct for errors due to fluctuations or drift in the instrument readings. The δ-values of the core sections in each batch of five were computed using *calculated* standard values determined by interpolation between the two *measured* standard values bracketing that particular series of sample values. For each isotope ratio the interpolated standard values were calculated by means of a linear regression formula relating the measured standard values to the relative time of analysis (i.e. the order in which the analyses were done) from the beginning to the end of the sequence of analyses. The δ-values of the reference samples were calculated using the standard data immediately preceding the sample data, as the standard was not reanalyzed after the analysis of the samples. Owing to financial constraints, the analyses were initially limited to core sections representing the depth range 0−15 cm, and this segment of the stratigraphic sequence was most intensively investigated. Additional isotope analyses were done a year later: The analyses of the two lowest sections in the original series (the 13−14 and 14−15 cm horizons) were repeated to check the previous results, and sections representing the depth range 15−20 cm were analyzed.

The chemical analysis of the sediments included determination of "reactive" (or "authigenic") manganese (Mn) and iron (Fe) by extraction with $NH_2OH\cdot HCl/HNO_3$ (*25*) and analysis of the extracts by inductively coupled atomic emission spectrometry using a Thermo Jarrell Ash IRIS unit. Reactive Mn and Fe comprise labile species (e.g. oxyhydroxides) that are subject to formation and transformation within a lake and its watershed by processes such as oxidation−reduction reactions, solubilization, and precipitation (*26*). Total carbon (C), organic C (all C remaining after removal of inorganic C by treatment with H_2SO_2), and organic nitrogen (N) were determined with a Perkin-Elmer 2400 CHN analyzer, and inorganic C content was calculated by subtracting organic C from total C.

The core sections were dated by the ^{210}Pb-^{210}Po method following measurement of porosity and specific gravity (*27−29*). The mean absolute age of each core section was calculated in accordance with the Constant Initial Concentration (CIC) model (*29−31*) and expressed as the estimated year of deposition.

TABLE 1. Radiometric Ages and Total Hg, $NH_2OH{\cdot}HCl/HNO_3$-Extractable Mn and Fe, and Organic C and N Concentrations of the Core Sections, and the N/C Ratio of the Organic Fraction[a]

depth (cm)	year (AD)	total Hg ($ng{\cdot}g^{-1}$)	$NH_2OH{\cdot}HCl/HNO_3$- extractable metals: Mn ($\mu g{\cdot}g^{-1}$)	Fe ($\mu g{\cdot}g^{-1}$)	Mn/Fe (wt/wt)	organic C (%)	organic N (%)	inorganic C (%)	N/C ratio of the organic matter (wt/wt)
0−1	1997 ± 7	46.4	53	1770	0.0301	2.18	0.12	0.43	0.055
1−2	1990 ± 7	46.7	52	1625	0.0320	2.14	0.11	0.51	0.051
2−3	1983 ± 7	48.2	56	1965	0.0285	2.25	0.11	0.40	0.049
3−4	1976 ± 7	49.8	58.5	1780	0.0329	2.27	0.08	0.49	0.035
4−5	1969 ± 6	44.7	61	1760	0.0347	2.23	0.11	0.46	0.049
5−6	1963 ± 6	45.6	59.5	1855	0.0322	2.24	0.12	0.46	0.054
6−7	1956 ± 7	44.8	62	1585	0.0391	2.25	0.10	0.45	0.044
7−8	1949 ± 7	44.3	68.5	1875	0.0374	2.32	0.13	0.39	0.056
8−9	1943 ± 7	45.9	107	1215	0.0880	2.33	0.10	0.46	0.043
9−10	1936 ± 7	44.6	76.5	1455	0.0529	2.46	0.09	0.32	0.037
10−11	1929 ± 7	41.6	86	1395	0.0622	2.53	0.14	0.23	0.055
11−12	1922 ± 7	43.1	65	1795	0.0362	2.25	0.14	0.47	0.062
12−13	1914 ± 8	42.8	58	2070	0.0286	1.79	0.10	0.92	0.056
13−14	1907 ± 8	43.4	59.5	1780	0.0343	2.32	0.12	0.44	0.052
14−15	1899 ± 8	38.6	52.5	1470	0.03575	2.27	0.12	0.31	0.053

[a] Age = approximate year of deposition. The Mn and Fe data are means for duplicate extracts; means ending in 0.5 (e.g. 58.5) were not rounded off. The C and N data were obtained by analysis of single samples. The samples were freeze-dried before being analyzed, and all element concentrations are based on dry weight.

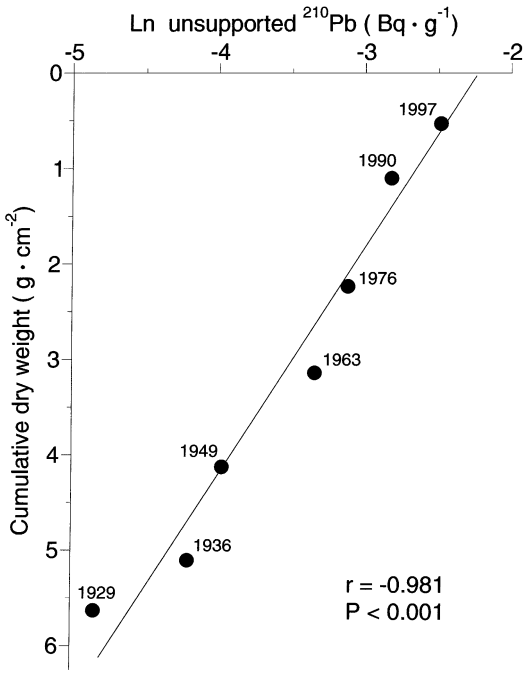

FIGURE 2. The relationship between unsupported ^{210}Pb and cumulative dry weight for selected core sections. Each point in the plot is accompanied by the corresponding year of deposition as calculated using the CIC model.

Results and Discussion

The Physical Properties and Chronology of the Core. The porosity of the core varied only slightly with depth (from 81.51% at the top to 70.45% at 15 cm), and the specific gravity was virtually constant (2.536, 2.528, and 2.531 $g{\cdot}cm^{-3}$ at 3, 8, and 13 cm, respectively), suggesting that the sediment's texture, composition, and rate of deposition scarcely changed from year to year (*29*). According to the radiometric dates, the core sections spanned the years 1899−1997 (Table 1). A plot of unsupported ^{210}Pb content against cumulative dry weight gave a highly significant inverse relationship, the points in the plot conforming closely to a single continuous trend (Figure 2). This implies that the orderly buildup of sediment strata over the years was never disrupted by processes such as bioturbation. The occurrence of fine laminations in the sediments and perpetual reducing conditions in the sediments and bottom water is also consistent with absence of bioturbation. Besides, the depth and stagnancy of the bottom water imply absence of erosion by currents and waves. We conclude that the core represented a continuous, undisturbed sequence of annual deposits.

Sediment Chemistry. Variations in the chemical composition of the core to a depth of 15 cm are shown in Table 1 and Figures 3 and 4. Total Hg content shows an overall tendency to increase from lower to higher (i.e. older to younger) horizons, with a mean enrichment factor of 1.34 for the four highest sections (in which the Hg levels were highest) relative to the lowest section (which had the lowest Hg level) (Figure 3). This trend is attributable to a progressive rise in annual emissions of Hg into the atmosphere from distant sources of pollution (*1−3, 21−24*). Comparable total Hg profiles supporting the same conclusion are commonly found in cores from widely separated localities in different parts of the world, including other High Arctic lakes (*21−24*). Total Hg varies independently of reactive Mn ($r = -0.0809$; $P \gg 0.1$), reactive Fe ($r = 0.254$; $P \gg 0.1$), and organic C ($r = -0.0922$; $P \gg 0.1$). Hence, there are no grounds for attributing the shape of the Hg profile to a temporal change in the composition or grain size frequency of the suspended matter deposited in the lake or to postdepositional redistribution of Hg, although evidence for this has been found in cores from certain other sites (*32−34*). Postdepositional solubilization and migration of trace quantities of Hg could have occurred, but if so, their overall effects have probably been negligible, as may be inferred from the high sedimentation rate in Romulus Lake (*21*) and the reasonable presumption that the Hg is strongly immobilized by sulfide and by thiol groups of organic matter under the perpetual reducing conditions that characterize the sedimentary environment (although immobilization of Hg under such conditions is by no means absolute) (*1*).

Hg Isotopes. The Hg isotope ratios for the core sections, standard solution, and reference samples (with the exception of the $^{196}Hg/^{202}Hg$ ratio, whose values, not surprisingly, were too low to be reliable (*5*)) are recorded in Table 2. The data show a high degree of precision (Table 2), as would be expected for results of MC-ICP-MS analysis. The precision is comparable to that of other workers' MC-ICP-MS data for Hg isotope ratios of meteorites (*15*) and cinnabar (*16, 17*).

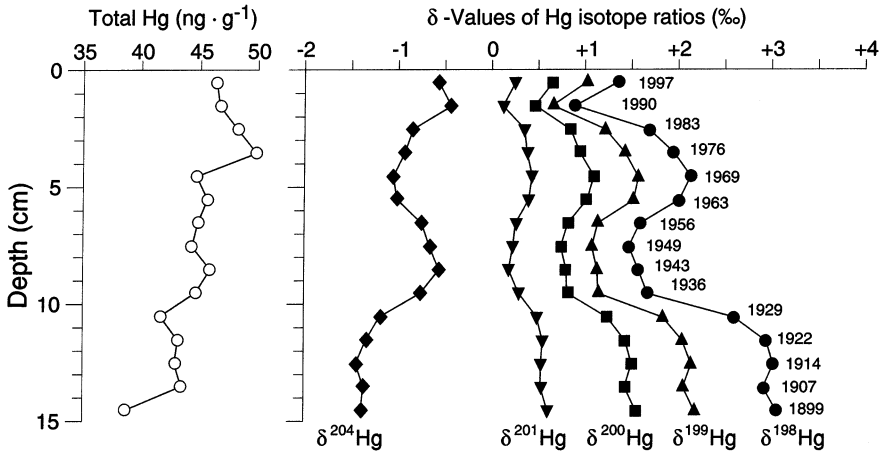

FIGURE 3. Variations in the total Hg concentrations and δ^{198}Hg, δ^{199}Hg, δ^{200}Hg, δ^{201}Hg, and δ^{204}Hg values with depth in the core down to a depth of 15 cm. The radiometric dates of the core sections are listed on the right.

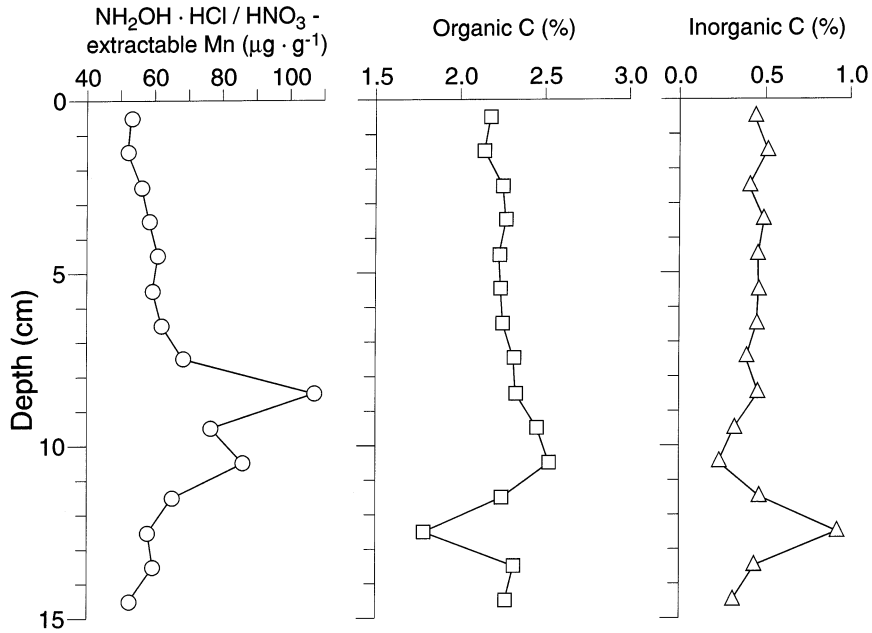

FIGURE 4. Variations in the $NH_2OH{\cdot}HCl/HNO_3$-extractable Mn, organic C, and inorganic C concentrations with depth in the core.

Moreover, ^{206}Pb, which is ~17 times more abundant than ^{204}Pb in nature, gave a signal that was 3 orders of magnitude lower than the ^{204}Hg signal, demonstrating that interference between ^{204}Pb and ^{204}Hg was negligible. The isotope ratios of the core sections differed significantly, systematically, and consistently from those of the standard (Table 2), as indicated by the corresponding δ-values (Table 3).

The δ^{198}Hg, δ^{199}Hg, δ^{200}Hg, δ^{201}Hg, and δ^{204}Hg values of the core sections (Table 3) vary in a complex but clearly nonrandom fashion with depth (i.e. with age) (Figure 3). The following regularities are immediately apparent: [i] Throughout the stratigraphic section the Hg is enriched in ^{198}Hg, ^{199}Hg, ^{200}Hg, and ^{201}Hg but correspondingly depleted in ^{204}Hg, relative to the Hg standard. [ii] The degree of enrichment conforms to the principle of mass bias, as it is an inverse function of atomic mass (decreasing in the order ^{198}Hg > ^{199}Hg > ^{200}Hg > ^{201}Hg, with ^{204}Hg showing negative enrichment, i.e., depletion). [iii] The Hg shows an overall tendency to become increasingly enriched in isotopes ^{198}Hg to ^{201}Hg and depleted in ^{204}Hg with increasing depth (i.e. age), the five lowest (pre-1936) core sections consistently showing the greatest degree of relative enrichment in ^{198}Hg, ^{199}Hg, ^{200}Hg, and ^{201}Hg and depletion in ^{204}Hg; but [iv] superimposed on this long-term trend is a series of large, regular shorter-term variations consisting of smoothly undulating alternate increases and decreases, all of which are of similar magnitude. The δ^{198}Hg, δ^{199}Hg, δ^{200}Hg, and δ^{201}Hg profiles parallel each other, and the δ^{204}Hg profile is a mirror image of them (providing further evidence that there was no significant interference by ^{204}Pb). The cause of the mass bias effect, which resulted in clean separation of the profiles (Table 3; Figure 3), is uncertain. Note that the δ-values of the reference substances differ markedly from those of the core sections immediately preceding them in the sequence of analyses and from one another (Table 3). This demonstrates that the isotope composition of Hg in various natural materials from different sources may differ appreciably, reflecting differences in the origin and history of the Hg.

The validity and reproducibility of the results for the core sections in the depth range 0−15 cm were strikingly confirmed in two respects by the supplementary analyses performed separately later (Table 3): [i] The δ-values for the repeat analyses of the 13−14 and 14−15 cm core sections agree very well with the original δ-values (except for the δ^{204}-Hg values, which vary widely and erratically in the second set of data, suggesting interference of unknown origin); and

TABLE 2. Hg Isotope Ratios of the Core Sections, Standard Solution, and Reference Samples[a,b]

	$^{198}Hg/^{202}Hg$		$^{199}Hg/^{202}Hg$		$^{200}Hg/^{202}Hg$		$^{201}Hg/^{202}Hg$		$^{204}Hg/^{202}Hg$	
sample	mean	SD	mean	SD	mean	SD	mean	SD	mean	SD
standard	0.327937	0.000009	0.557489	0.000012	0.767012	0.000016	0.439878	0.000004	0.232502	0.000004
core, 0−1	0.328336	0.000022	0.557993	0.000019	0.767461	0.000024	0.439973	0.000004	0.232390	0.000011
core, 1−2	0.328141	0.000029	0.557733	0.000008	0.767255	0.000027	0.439902	0.000018	0.232442	0.000028
core, 2−3	0.328353	0.000009	0.557986	0.000007	0.767488	0.000015	0.439987	0.000006	0.232368	0.000010
core, 3−4	0.328396	0.000015	0.558047	0.000013	0.767520	0.000013	0.439986	0.000006	0.232369	0.000010
core, 4−5	0.328413	0.000022	0.558066	0.000013	0.767579	0.000010	0.439992	0.000008	0.232355	0.000006
standard	0.327670	0.000012	0.557134	0.000018	0.766678	0.000016	0.439789	0.000011	0.232627	0.000015
core, 5−6	0.328339	0.000013	0.558001	0.000019	0.767477	0.000012	0.439972	0.000013	0.232384	0.000009
core, 6−7	0.328211	0.000054	0.557798	0.000066	0.767340	0.000055	0.439922	0.000017	0.232437	0.000024
core, 7−8	0.328183	0.000021	0.557782	0.000029	0.767304	0.000022	0.439915	0.000011	0.232451	0.000007
core, 8−9	0.328224	0.000043	0.557833	0.000055	0.767363	0.000038	0.439901	0.000013	0.232467	0.000037
core, 9−10	0.328269	0.000012	0.557862	0.000010	0.767391	0.000019	0.439958	0.000005	0.232415	0.000009
standard	0.327731	0.000010	0.557240	0.000022	0.766781	0.000025	0.439839	0.000013	0.232585	0.000004
core, 10−11	0.328642	0.000005	0.558336	0.000015	0.767799	0.000012	0.440067	0.000016	0.232283	0.000010
core, 11−12	0.328819	0.000011	0.558524	0.000023	0.768016	0.000026	0.440109	0.000011	0.232228	0.000009
core, 12−13	0.328901	0.000007	0.558650	0.000009	0.768137	0.000021	0.440117	0.000014	0.232177	0.000008
core, 13−14	0.328930	0.000016	0.558676	0.000016	0.768150	0.000021	0.440129	0.000019	0.232173	0.000009
core, 14−15	0.329037	0.000007	0.558820	0.000012	0.768302	0.000013	0.440176	0.000008	0.232146	0.000009
standard	0.328097	0.000012	0.557684	0.000015	0.767192	0.000018	0.439925	0.000019	0.232447	0.000005
ref SO-2	0.328541	0.000055	0.557993	0.000096	0.767757	0.000089	0.439896	0.000030	0.232644	0.000390
ref GXR-2	0.328188	0.000008	0.557740	0.000009	0.767291	0.000012	0.439934	0.000006	0.232434	0.000003
ref GXR-4	0.328586	0.000035	0.558362	0.000047	0.767777	0.000030	0.440128	0.000020	0.232252	0.000011

[a] Explanation of terms: "core" followed by two numbers separated by a hyphen = core section identified by depth range in cm; "ref" = reference sample; SD = standard deviation. [b] Each value in the table is based on data for 25 replicate analyses performed in rapid succession on a single solution. To estimate the analytical error, calculate either the standard error (= SD/$\sqrt{25}$) or the 95% confidence limit of the mean (= $t_{0.95}$SD/$\sqrt{25}$, where $t_{0.95}$ = Student's t for 95% confidence = 2.064 for 24 degrees of freedom) (*19*). The parameter 2SE, where SE = standard error, has been used as an approximation of the 95% confidence limit.

TABLE 3. δ-Values for the $^{198}Hg/^{202}Hg$, $^{199}Hg/^{202}Hg$, $^{200}Hg/^{202}Hg$, $^{201}Hg/^{202}Hg$, and $^{204}Hg/^{202}Hg$ Ratios of the Core Sections and Reference Samples[a,b]

sample	$\delta^{198}Hg$	$\delta^{199}Hg$	$\delta^{200}Hg$	$\delta^{201}Hg$	$\delta^{204}Hg$
			Series 1		
core, 0−1	+1.35258	+1.00999	+0.658056	+0.249623	−0.571986
core, 1−2	+0.893707	+0.649478	+0.461989	+0.122088	−0.438627
core, 2−3	+1.67631	+1.21117	+0.838501	+0.348996	−0.842779
core, 3−4	+1.94350	+1.42664	+0.952935	+0.380384	−0.928693
core, 4−5	+2.13143	+1.56678	+1.10247	+0.427918	−1.06329
core, 5−6	+2.01059	+1.52382	+1.01970	+0.397228	−1.01453
core, 6−7	+1.58891	+1.12892	+0.818690	+0.264435	−0.756622
core, 7−8	+1.47238	+1.06786	+0.749286	+0.229643	−0.666363
core, 8−9	+1.56632	+1.12705	+0.803786	+0.179163	−0.567500
core, 9−10	+1.67277	+1.14855	+0.817983	+0.289430	−0.760989
core, 10−11	+2.59311	+1.83380	+1.23818	+0.485844	−1.19968
core, 11−12	+2.94644	+2.03808	+1.43170	+0.548574	−1.33741
core, 12−13	+3.00994	+2.13109	+1.50003	+0.534234	−1.45796
core, 13−14	+2.91181	+2.04471	+1.42754	+0.528988	−1.37639
core, 14−15	+3.05149	+2.16998	+1.53626	+0.603077	−1.39373
ref SO-2	+1.35326	+0.554077	+0.736452	−0.0659203	+0.847505
ref GXR-2	+0.277357	+0.100415	+0.129042	+0.0204580	−0.0559267
ref GXR-4	+1.49041	+1.21574	+0.762521	+0.461442	−0.838901
			Series 2		
core, 13−14 (R)	+2.58936	+2.02456	+1.28089	+0.639562	−3.76240
core, 14−15 (R)	+2.64274	+2.36192	+1.44695	+0.773515	+0.131061
core, 15−16	+2.77050	+2.22848	+1.59904	+0.704691	−7.67690
core, 16−17	+2.81110	+2.43041	+1.54323	+0.977971	−9.49451
core, 17−18	+1.35116	+1.16373	+0.678208	+0.229753	−6.69032
core, 18−19	+2.26458	+1.54760	+0.991682	+0.410749	+2.04974
core, 19−20	+3.06753	+2.44174	+1.37112	+0.891858	−10.2747

[a] Explanation of sample designations: Same as in footnote *a* of Table 2. "Series 1" comprises the samples analyzed initially (core sections 0−1 to 14−15 and the reference samples); "Series 2" consists of additional core samples (duplicate portions of sections 13−14 and 14−15 in Series 1, together with horizons 15−16 to 19−20) which were analyzed separately the following year. "R" signifies repetition of previous analyses. [b] δ-values are per mil (‰) deviations with respect to the standard.

[ii] the sequence of consistently high δ-values for the four lightest isotopes (^{198}Hg to ^{201}Hg) in the 10−15 cm depth range extends without interruption into the 15−16 and 16−17 cm horizons, indicating continuity with the pattern of variation revealed by the earlier data. (Below the 16−17 cm horizon the δ-values decline sharply to a minimum and then rise again, but, as usual, the regularity of this feature rules out random fluctuation.)

The δ-values as a whole correlate significantly with total Hg (e.g. for δ^{199}Hg, $r = -0.706$; $P > 0.001$, < 0.01), because

they, like total Hg, show long-term overall tendencies, but the relationships are partly obscured by the prominent shorter-term variations. One possible explanation for the correlation is that relict isotope signatures inherited from the sources of Hg contamination have been at least partially preserved. This hypothesis is based on the assumption that the anthropogenic component of the Hg has a different isotopic makeup than the component derived from natural sources and that the temporal increase in anthropogenic Hg inferred from the total Hg profile was accompanied by a corresponding shift in isotope composition represented, in particular, by the parallel overall trends of the δ-values. An equally plausible alternative explanation, however, is that the Hg isotopes were fractionated by natural processes in the environment and that the trends reflect long-term environmental changes which affected isotope fractionation and happened to parallel the temporal rise in the rate of Hg pollution.

The shorter-term variations which are superimposed on the overall trends of the δ-values, in large part obscuring them (Figure 3), are also consistent with in situ fractionation of the Hg isotopes. As they are unrelated to variations in total Hg concentration (Figure 3), they do not provide evidence for preservation of isotope signatures carried over from particular sources of contamination; yet this in itself does not disprove the presence of source-related effects, as maxima and minima of the kind seen in the profiles of the δ-values could, in theory, have been produced by temporal variations in the percent contributions from different sources of Hg (owing to variations in rates of emission, or atmospheric factors such as wind direction, or both) irrespective of the overall Hg loading. Comparison of these features with corresponding regions of a high-resolution Hg profile representing a record of atmospheric Hg deposition in a dated ice core from a glacier in Wyoming (*35*), and with temporal variations in global Hg production (*35*), revealed suggestive, though inconclusive, similarities, implying that effects of source-related isotope signatures, though unproven, cannot be ruled out. The following features of the ice core's Hg profile correspond to a greater or lesser extent with characteristic features of the Hg isotope profiles: [i] a small peak spanning the years ca. 1905−1920; [ii] a larger peak that spans the years ca. 1930−1945; and [iii] the largest peak, which rises steadily from ca. 1950 to 1990 and then declines sharply. In addition, there were two major intervals of elevated global Hg production that could be linked to the variations in isotope composition, one spanning the period ca. 1933−1948 and peaking in 1940, and the other extending across the years ca. 1948−1990 and reaching its maximum in 1970; a smaller maximum in the interval ca. 1920−1933 does not correspond to any of the features of the isotope data. The 1970 maximum of global Hg production and the abrupt decline in ice core Hg levels after 1990 provide the best match with the profiles of the isotope data. The other resemblances are less exact and hence less convincing. In any event, the points of resemblance, though suggestive, do not necessarily denote preservation of source-related isotope signatures in the lake sediments: They could merely mean that Hg pollution tended to correlate with other environmental changes (*2*) which affected processes that cause fractionation of Hg isotopes in the lake. A more telling argument against preservation of detectable isotope signatures inherited from the sources of pollution is the fact that the sequential variations in isotope composition are of comparable magnitude (Figure 3), whereas the roughly equivalent maxima of the ice core's Hg profile differ greatly in size (*35*).

Plots of δ-values against reactive Mn concentration yielded important clues to the causes of the observed temporal variations in the isotopic makeup of the Hg and greatly strengthened the case for fractionation of Hg isotopes in the environment. The plot for δ^{199}Hg (Figure 5) is a good example for purposes of illustration, although δ^{198}Hg, δ^{200}Hg, and δ^{201}Hg gave essentially the same result, and δ^{204}Hg shows the same variations in reverse (Tables 1 and 3). The points in the plot resolve themselves into three separate and distinct groups, revealing clear-cut differentiation of the sediment sequence into three radically different domains: the oldest (1899−1929), intermediate (1936−1956), and youngest (1963−1997) horizons, representing depths of 10−15, 6−10, and 0−6 cm, respectively. The δ^{199}Hg values of the five oldest core sections, besides being consistently higher than those of the younger parts of the core, give a highly significant *inverse* correlation with reactive Mn; in contrast, the δ^{199}Hg values of the six youngest sections show a highly significant *positive* correlation. Thus, Hg becomes isotopically heavier with increasing reactive Mn in the oldest deposits but lighter in the most recent deposits. In the same two regions of the core, however, total Hg varies independently of reactive Mn ($r = -0.195$, $P \gg 0.1$ for 0−6 cm; $r = 0.273$, $P \gg 0.1$ for 10−15 cm), and, accordingly, δ^{199}Hg varies independently of total Hg ($r = -0.164$, $P \gg 0.1$ for 0−6 cm; $r = -0.295$, $P \gg 0.1$ for 10−15 cm). The δ^{199}Hg values of the four intermediate sections are nearly constant and are independent of reactive Mn, yielding a virtually horizontal regression line. This suggests that the diametrically opposed tendencies in the oldest and youngest regions are equally developed and therefore cancel each other, in the intervening region. Similar relationships were observed when the δ-values were plotted against organic C concentration (Tables 1 and 3), but it was obvious from inspection that the correlations were weaker. In contrast, the δ-values (Table 3) vary independently of reactive Fe (Table 1), although the Mn/Fe ratio of the reactive fraction (Table 1) gives nearly the same results as reactive Mn. Evidently the variations in the isotope composition of Hg are primarily linked to reactive Mn or to the biogeochemical processes that controlled its abundance.

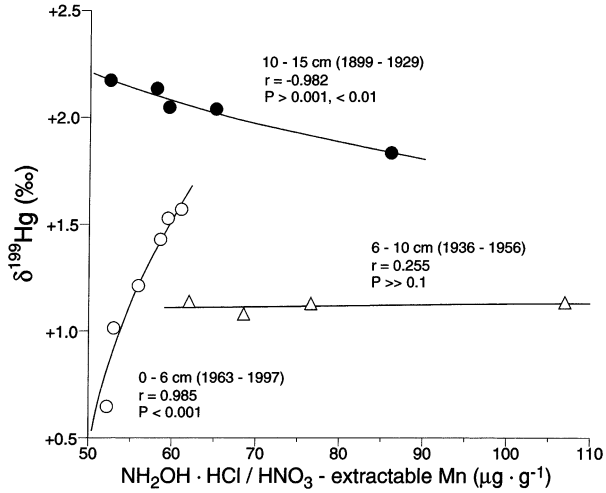

FIGURE 5. The relationships between δ^{199}Hg and $NH_2OH{\cdot}HCl/HNO_3$-extractable Mn concentration in core sections representing depths of 0−6 cm (○), 6−10 cm (△), and 10−15 cm (●).

The variations in the δ-values of the Hg isotope ratios as functions of the reactive Mn content, Mn/Fe ratio, and organic C content of the sediment suggest fractionation of Hg isotopes by natural processes in the environment, as they relate changes in the isotopic makeup of the Hg to independent evidence for local environmental and biogeochemical changes. Fractionation of Hg isotopes in the environment has probably obliterated whatever isotope signatures were imprinted on the Hg at its points of origin, although the results do not exclude the possibility that traces of source-

related signatures have been preserved. Moreover, the relationships between δ-values and sediment chemistry provide further evidence that the variations in isotope composition are inherent characteristics of the Hg. It is extremely unlikely that the striking, highly significant relationships shown in Figure 5 were produced by random variation or artifacts.

More research is needed to explain the relationships between the isotopic makeup of the Hg and the reactive Mn levels. This would have to include a more detailed investigation of the biogeochemistry of Mn in the lake and its watershed, as the distribution of reactive Mn in a core may be a function of many interrelated factors, including oxidation−reduction reactions, pH, the ionic composition of the water, primary production, and microbial activities, and could reflect conditions in the watershed (e.g. the waterlogging of soil, causing release of dissolved Mn(II) into the lake) as well as in the lake itself (*26, 36, 37*). Meanwhile, a reasonable working hypothesis based on the available evidence would be that the postulated fractionation of Hg isotopes was largely or wholly the result of microbial activities involved in oxidation−reduction reactions, as appears to have been the case in Lake Ontario (*4*), and could have occurred in the water column or the sediments, or both, and possibly in the watershed as well. The fact that the variations in the Hg isotope data are linked to organic C as well as reactive Mn is consistent with a key role for biological activity. Thus, phytoplankton, by producing labile organic matter and stimulating the growth of heterotrophic bacteria, would tend to promote the reduction and mobilization of Mn. The specific forms of the reactive Mn in the sediment cannot be identified from the evidence presented here, but, considering the perpetually reducing conditions in the sediments and bottom water, they probably consist chiefly or entirely of Mn(II) species, such as Mn^{2+} ions and complexes dissolved in interstitial water and sorbed by particles, together with solid phases such as MnS and $MnCO_3$ (*26, 38*). Any dissolved Mn(II) diffusing upward through the anoxic hypolimnion is presumably oxidized and precipitated as MnOOH on coming into contact with O_2-rich epilimnetic waters (*26, 38, 39*), whereupon the MnOOH settles out and is partially or completely reduced and solubilized on sinking into the anoxic zone (*26, 40*). Oxidation and reduction of the Mn are probably mediated directly and indirectly by bacteria (*37, 41, 42*).

The reversal of the relationships between the δ-values of the Hg isotope ratios and the reactive Mn concentrations from the base of the core to the top (Figure 5) suggests a change from one biogeochemical regime to another in the course of time. Thus, the sediment sequence appears to be divided into three distinct biogeochemical zones with sharp boundaries between them, the intermediate one being a transition zone between the other two. The systematic temporal variation in the nature of the relationship between the isotope composition of Hg and the reactive Mn concentration is consistent with progressive long-term environmental change accompanied by corresponding successional changes in the species composition, and hence the isotope-fractionating activities, of the microbial community (*4, 43−46*). The sharp boundaries dividing the core cleanly into the three zones defined by relationships between the δ-values and the reactive Mn are surprising, but they may denote the existence of critical threshold conditions beyond which the taxonomic makeup of the microflora changed rapidly and dramatically. The postulated environmental change could have been due to an increase in the annual loadings of airborne pollutants, including Hg itself (Figure 3), other heavy metals, radionuclides, strong acids produced by fossil fuel combustion, and persistent xenobiotic organic compounds, which are known to have increased during the same period (*47−50*). Another possible explanation is a well documented warming trend in the Arctic that started in the 19th century and continued in the 20th, leading to increased biological productivity, changes in the nature of the biota (e.g. the species composition of the planktonic diatom flora), and a rise in annual rates of sedimentation in certain Arctic lakes (*51−57*), presumably causing successional changes in the species composition of the bacterial community (*43−46*). In Romulus Lake a general increase in productivity over time is unlikely, as organic C peaks at ~10−11 cm and then *decreases* upward (Table 1; Figure 4), and the core's relatively uniform physical properties are not consistent with a temporal rise in the annual rate of sedimentation. Nonetheless, climatic warming could have altered the species makeup of the biota. In brief, the available evidence suggests environmentally and microbially controlled fractionation of Hg isotopes. The variations in isotope composition could be due to long-term temporal change in environmental conditions and related changes in the nature of the biota, possibly reflecting the combined effects of many different factors.

The core profiles of reactive Mn, organic C, and inorganic C (Figure 4) show that certain shorter-term changes in environmental conditions and microbial activities may also be regarded as possible causes of the temporal changes in the relationship between Hg isotope composition and sediment chemistry (Figure 5) or as contributing factors. Shorter-term changes in local conditions and longer-term large-scale environmental trends are not mutually exclusive; the former could be superimposed on the latter, producing a complex interactive effect. Reactive Mn increases upward from 15 to 10 cm and then, reversing itself at ~10 cm, tends to decrease steadily upward to the top of the core except for interruption of the trend by a large maximum superimposed on it in the depth range 8−9 cm. It is particularly noteworthy that the reactive Mn trend in the 10−15 cm depth interval coincides with the zone in which the δ-values for isotopes ^{198}Hg to ^{201}Hg decrease with increasing reactive Mn and that reversal of the reactive Mn trend immediately above this region is accompanied by an abrupt change in the relationship between Hg isotope composition and reactive Mn (Figure 5). The organic C profile parallels the reactive Mn profile except that it [i] has a prominent minimum at 12−13 cm which is barely reflected in the reactive Mn profile and [ii] has no feature corresponding to the reactive Mn peak at 8−9 cm. Not counting these two anomalies, there is a highly significant positive correlation between reactive Mn and organic C ($r = 0.923$; $P < 0.001$), presumably reflecting the role of biological activity and organic matter in oxidation−reduction reactions and Mn chemistry in the lake. As the anomalous enrichment in reactive Mn in the 8−9 cm depth interval is unrelated to organic C concentration, it is probably independent of biological productivity and isotope-fractionating processes in the lake. It may well have resulted from an episodic event in the watershed, such as temporary saturation of soil with meltwater ponded by the impervious underlying layer of permafrost (*20*), leading to development of anoxic conditions and release of dissolved Mn(II) into runoff flowing into the lake (*26*). However, this short-lived aberration has no bearing on the general validity of our tentative interpretation of the relationships between the Hg isotope and reactive Mn data (Figure 5). Besides, the 8−9 cm interval in which the Mn anomaly occurs falls within the depth range (6−10 cm) in which isotope composition is independent of reactive Mn and is nearly constant (Figure 5). As for the organic C minimum at 12−13 cm, it could signify a temporary drop in primary production owing to short-term environmental change. Inorganic C is inversely related to organic C, suggesting photosynthetic production of organic matter at the expense of dissolved inorganic C in the epilimnion or dilution of inorganic C by organic C in the sediment. Organic N and the N/C ratio (Table 1) show only

minor, seemingly random variation, implying absence of appreciable change in the proportion of allochthonous to autochthonous organic matter but not ruling out variation in the nature of the aquatic biota. Most of the organic matter is probably autochthonous, as the surrounding land has scant vegetation.

Implications and Suggestions for Future Research. The findings reported here, along with the results published earlier (*4*), have opened up a new and potentially fruitful, but heretofore neglected, area of research on Hg in the environment. They demonstrate that hitherto unknown systematic variations in the stable isotope composition of Hg, together with related physicochemical and biological data, could yield much valuable untapped information about the biogeochemical cycling of Hg. In the future there will be a need for in-depth interdisciplinary research employing a variety of methods to follow up on this promising beginning. A key question that needs to be resolved is whether Hg emissions from different natural and anthropogenic sources have characteristic isotope signatures indicative of their origin, and, if so, what happens to them after the Hg is released into the environment: Are they invariably obliterated by isotope fractionation (and obscured by the mixing of emissions from different sources), or can they be at least partially preserved? Another important objective will be to elucidate the mechanisms and results of Hg isotope fractionation by various physical, chemical, and biological processes in the environment.

Thus, isotope ratios of Hg from different anthropogenic and natural point sources should be compared, and possible alteration of these ratios in various well-defined natural environments should be investigated. Sediments, water, and organisms from aquatic ecosystems representing widely differing environmental regimes, biotas, geographical locations, and sources of contamination, along with terrestrial and atmospheric samples, should be analyzed for the purpose of discerning broad tendencies and patterns of variation that might lead to generalizations about the processes responsible for empirically observed temporal and spatial variations in isotope ratios. It will be necessary to collect not only Hg isotope data but also a wide range of related data that may provide clues to the processes that cause fractionation of the isotopes. In the analysis of core sections, this would include information on environmentally diagnostic microfossils as well as chemical and mineralogical composition, physical properties, pollutants other than Hg, and radiometric ages. A useful strategy would be to analyze samples collected at different distances from known sources of Hg or in different environments polluted with Hg from a single source. Ideally, different forms of Hg, such as Hg(0), inorganic Hg(II), and methyl Hg, should be analyzed separately. Another potentially fruitful approach would be to combine analysis of field samples with controlled experiments to investigate the processes and specific mechanisms of Hg isotope fractionation in nature. Finally, experiments are needed to detect and eliminate any artifacts that might be produced during sample storage, preparation, extraction, or analysis—e.g. loss of volatile Hg species during freeze-drying (although this is not likely to be quantitatively significant for sediment samples) or interaction of Hg with other components of the samples during digestion.

Acknowledgments

Initially the research was done in collaboration with the late V. Cheam (National Water Research Institute (NWRI), Burlington, Ontario). We thank C. Belzile and P. van Hove (Université Laval, Québec) for assistance in the field, R. Pienitz (Université Laval) for the use of sampling equipment, and the Polar Continental Shelf Project for logistic support. The total Hg and Hg isotope analyses were performed by Activation Laboratories Ltd. (Ancaster, Ontario) under the direction of Y. Kapusta using methods developed by the company. The Mn and Fe were extracted by N. Nguyen (NWRI), and the Mn, Fe, C, and N analyses were done by the National Laboratory for Environmental Testing at NWRI under the direction of G. Sardella. The radiometric dates and physical properties of the sediments were determined by F. Yang (NWRI). A. El-Shaarawi (NWRI) kindly supplied advice and information about statistics. The project was funded by the Northern Contaminants Program of Indian and Northern Affairs Canada and the Natural Sciences and Engineering Research Council of Canada.

Literature Cited

(1) Jackson, T. A. In *Metal Metabolism in Aquatic Environments*; Langston, W. J., Bebianno, M. J., Eds.; Chapman & Hall: London, 1998; pp 77−158.
(2) Jackson, T. A. *Environ. Rev.* **1997**, *5*, 99−120 and 207.
(3) Fitzgerald, W. F.; Engstrom, D. R.; Mason, R. P.; Nater, E. A. *Environ. Sci. Technol.* **1998**, *32*, 1−7.
(4) Jackson, T. A. *Can. J. Fish. Aquat. Sci.* **2001**, *58*, 185−196.
(5) De Bièvre, P.; Taylor, P. D. P. *Int. J. Mass Spectrom. Ion Proc.* **1993**, *123*, 149−166.
(6) Brönsted, J. N.; von Hevesy, G. *Z. Phys. Chem.* **1921**, *99*, 189−206.
(7) Mulliken, R. S.; Harkins, W. D. *J. Am. Chem. Soc.* **1922**, *44*, 37−65.
(8) Haeffner, E. *Nature* **1953**, *172*, 775−776.
(9) Obelenskii, A. A.; Doilnitsyn, Y. F. *Dokl. Akad. Nauk SSSR* **1976**, *230*, 701−704.
(10) Koval, N. A.; Zakharchenko, V. V.; Savin, O. R.; Vinogradov, V. I.; Shkurdoda, V. A.; Simonovskii, V. I. *Dokl. Akad. Nauk SSSR* **1977**, *235*, 936−938.
(11) Kuznetsov, V. V.; Obolenskii, A. A. *Dokl. Akad. Nauk SSSR* **1980**, *252*, 459−460.
(12) Jovanovic, S.; Reed, G. W., Jr. *Chem. Geol.* **1990**, *80*, 181−191.
(13) Kumar, P.; Goel, P. S. *Geochem. J.* **1992**, *26*, 51−61.
(14) Kumar, P.; Goel, P. S. *Chem. Geol.* **1992**, *102*, 171−183.
(15) Lauretta, D. S.; Klaue, B.; Blum, J. D.; Buseck, P. R. *Geochim. Cosmochim. Acta* **2001**, *65*, 2807−2818.
(16) Hintelmann, H.; Lu, S. Y. *Analyst* **2003**, 635−639.
(17) Evans, R. D.; Hintelmann, H.; Dillon, P. J. *J. Anal. At. Spectrom.* **2001**, *16*, 1064−1069.
(18) Hintelmann, H.; Dillon, P.; Evans, R. D.; Rudd, J. W. M.; Bodaly, R. A. *Can. J. Fish. Aquat. Sci.* **2001**, *58*, 2309−2311.
(19) Jackson, T. A. *Can. J. Fish. Aquat. Sci.* **2001**, *58*, 2312−2316.
(20) Davidge, G. D. *Physical Limnology and Sedimentology of Romulus Lake: A Meromictic Lake in the Canadian High Arctic*; M.Sc. Thesis, Queen's University, Kingston, Ontario, Canada, 1994.
(21) Muir, D.; Halliwell, D.; Cheam, V. *Spatial trends in loadings and historical inputs of mercury inferred from pan-Northern lake sediment cores*; Report to Northern Ecosystem Initiative; NEI Secretariat, Environment Canada, Yellowknife, Northwest Territories, Canada, 15 pp.
(22) Lockhart, W. L.; Wilkinson, P.; Billeck, B. N.; Hunt, R. V.; Wagemann, R.; Brunskill, G. L. *Water, Air, Soil Pollut.* **1995**, *80*, 603−610.
(23) Lockhart, W. L.; Wilkinson, P.; Billeck, B. N.; Danell, R. A.; Hunt, R. V.; Brunskill, G. J.; Delaronde, J.; St. Louis, V. *Biogeochem.* **1998**, *40*, 163−173.
(24) Bindler, R.; Renberg, I.; Appleby, P. G.; Anderson, N. J.; Rose, N. L. *Environ. Sci. Technol.* **2001**, *35*, 1736−1741.
(25) Chao, T. T. *Soil Sci. Soc. Am. Proc.* **1972**, *36*, 764−768.
(26) Engstrom, D. R.; Wright, H. E., Jr. In *Lake Sediments and Environmental History*; Haworth, E. Y., Lund, J. W. G., Eds.; University of Minnesota Press: Minneapolis, 1984; pp 11−67.
(27) Eakins, J. D.; Morrison, R. T. *Int. J. Appl. Radiat. Isotopes* **1978**, *29*, 531−536.
(28) Turner, L. J. *Laboratory Determination of ^{210}Pb − ^{210}Po Using Alpha Spectrometry*, 2nd ed.; Tech. Note 90-TN-07; National Water Research Institute: Burlington, Ontario, Canada, 1990.
(29) Yang, F. *^{210}Pb Dating of Lacustrine Sediments from Lake Romulus (Core 228), SW Ellesmere*; NWRI Report 2001-01; National Water Research Institute: Burlington, Ontario, Canada, 2001.
(30) Matsumoto, E. *Geochem. J.* **1975**, *9*, 167−172.
(31) Robbins, J. A.; Edgington, D. N. *Geochim. Cosmochim. Acta* **1975**, *39*, 285−304.
(32) Gobeil, C.; Cossa, D. *Can. J. Fish. Aquat. Sci.* **1993**, *50*, 1794−1800.

(33) Gobeil, C.; MacDonald, R. W.; Smith, J. N. *Environ. Sci. Technol.* **1999**, *33*, 4194−4198.
(34) Matty, J. M.; Long, D. T. *J. Great Lakes Res.* **1995**, *21*, 574−586.
(35) Schuster, P. F.; Krabbenhoft, D. P.; Naftz, D. L.; Cecil, L. D.; Olson, M. L.; Dewild, J. F.; Susong, D. D.; Green, J. R.; Abbott, M. L. *Environ. Sci. Technol.* **2002**, *36*, 2303−2310.
(36) Engstrom, D. R.; Swain, E. B.; Kingston, J. C. *Freshwater Biol.* **1985**, *15*, 261−288.
(37) Kjensmo, J. *Arch. Hydrobiol.* **1968**, *65*, 125−141.
(38) Santschi, P.; Höhener, P.; Benoit, G.; Buchholtz-ten Brink, M. *Marine Chem.* **1990**, *30*, 269−315.
(39) Jackson, T. A.; Bistricki, T. *J. Geochem. Explor.* **1995**, *52*, 97−125.
(40) Davison, W.; Woof, C.; Rigg, E. *Limnol. Oceanogr.* **1982**, *27*, 987−1003.
(41) Nealson, K. H.; Rosson, R. A.; Myers, C. R. In *Metal Ions and Bacteria*; Beveridge, T. J., Doyle, R. J., Eds.; John Wiley & Sons: New York, 1989; pp 383−411.
(42) Johnston, C. G.; Kipphut, G. W. *Appl. Environ. Microbiol.* **1988**, *54*, 1440−1445.
(43) Jackson, T. A. In *Heavy Metals in the Environment*; (Proc. Internat. Conf., Toronto, Sept., 1993); Allan, R. J., Nriagu, J. O., Eds.; CEP Consultants Ltd.: Edinburgh, 1993; Vol. 2, pp 301−304.
(44) Jackson, T. A. *Appl. Organomet. Chem.* **1989**, *3*, 1−30.
(45) Jackson, T. A. *Can. J. Fish. Aquat. Sci.* **1991**, *48*, 2449−2470.
(46) Jackson, T. A. In *Heavy Metals in the Environment*; Vernet, J.-P., Ed.; Elsevier: Amsterdam, 1991; pp 191−217.
(47) Kerr, R. A. *Science* **1981**, *212*, 1013−1014.
(48) Koerner, R. M.; Fisher, D. *Nature* **1982**, *295*, 137−140.
(49) Barrie, L. A.; Gregor, D.; Hargrave, B.; Lake, R.; Muir, D.; Shearer, R.; Tracey, B.; Bidleman, T. *Sci. Total Environ.* **1992**, *122*, 1−74.
(50) Muir, D. C. G.; Omelchenko, A.; Grift, N. P.; Savoie, D. A.; Lockhart, W. L.; Wilkinson, P.; Brunskill, G. J. *Environ. Sci. Technol.* **1996**, *30*, 3609−3617.
(51) Koerner, R. M.; Fisher, D. A. *Nature* **1990**, *343*, 630−631.
(52) Douglas, M. S. V.; Smol, J. P.; Blake, W., Jr. *Science* **1994**, *266*, 416−419.
(53) Gajewski, K.; Hamilton, P. B.; McNeely, R. *J. Paleolimnol.* **1997**, *17*, 215−225.
(54) Overpeck, J.; Hughen, K.; Hardy, D.; Bradley, R.; Case, R.; Douglas, M.; Finney, B.; Gajewski, K.; Jacoby, G.; Jennings, A.; Lamoureux, S.; Lasca, A.; MacDonald, G.; Moore, J.; Retelle, M.; Smith, S.; Wolfe, A.; Zielinski, G. *Science* **1997**, *278*, 1251−1256.
(55) Hughen, K. A.; Overpeck, J. T.; Anderson, R. F. *Holocene* **2000**, *10*, 9−19.
(56) Smol, J. P.; Cumming, B. F. *J. Phycol.* **2000**, *36*, 986−1011.
(57) Joynt, E. H., III; Wolfe, A. P. *Can. J. Fish. Aquat. Sci.* **2001**, *58*, 1222−1243.

Received for review August 18, 2003. Accepted February 27, 2004.

ES0306009